# Stability of semidiscrete formulations for elastodynamics at small time steps

Eran Grosu, Isaac Harari

# Stability of semidiscrete formulations for elastodynamics at small time steps

Eran Grosu, Isaac Harari*

*Department of Solid Mechanics, Materials, and Systems, Tel Aviv University, 69978 Ramat Aviv, Israel*

Solutions of direct time-integration schemes for elastodynamics that converge in time to conventional semidiscrete formulations may be polluted at small time steps by spurious oscillations that violate the principle of causality, for example by arising before wave fronts. This degradation is not an artifact of the time-marching scheme, but rather a property of the solution of the semidiscrete formulation itself. An analogy to singularly perturbed elliptic problems provides an upper bound on the time step for the onset of these oscillations. A simple procedure of spatial stabilization is proposed to remove this pathology from implicit time-integration schemes, without affecting unconditional temporal stability. Spatially stabilized implicit time-integration methods are free of noncausal oscillations at small time steps.

*Keywords:* Semidiscrete; Small time step oscillation; Rothe method; Spatial stabilization; Principle of causality

## 1. Introduction

Dynamic behavior of elastic bodies (elastodynamics) is described by the equation of motion, which is continuous in space and time. Finite element methods are usually used to obtain numerical solutions for problems in structural dynamics.

The common approach to transient computation (the method of lines [1]) is time-integration of a semidiscrete formulation, which is obtained by spatial discretization. Thus, the approximation is carried out in two stages. First, spatial approximation, e.g., by standard finite element methods, leads to the semidiscrete formulation (a coupled system of ordinary differential equations in time). Then, temporal discretization by time-integration schemes results in a system of algebraic equations at each time level. Perhaps the most widely used family of direct methods for solving the semidiscrete equation of motion is the Newmark family of methods for time-integration. The unconditionally stable in time, second-order accurate trapezoidal rule is, probably, the most commonly used implicit algorithm among the Newmark family.

* Corresponding author. Tel.: +972 3 640 9439; fax: +972 3 640 8158.
*E-mail address:* harari@eng.tau.ac.il (I. Harari).
*URL:* http://www.eng.tau.ac.il/∼harari

It is well known that higher modes, related to higher frequencies of semidiscrete formulations, are approximated poorly [2, Section 6.3]. As a result, algorithmic damping is often introduced in time-integration schemes in order to remove participation of high-frequency modal components [3,4]. Algorithmic damping cannot be introduced in the Newmark method without degrading the order of accuracy. Hence, the trapezoidal rule lacks algorithmic damping. The implicit, unconditionally stable in time, second-order accurate HHT-$\alpha$ [3] and generalized-$\alpha$ [4] algorithms are extensions of the Newmark method with adjustable algorithmic damping introduced to improve this shortcoming.

Conventional wisdom advocates that time step reduction be accompanied by corresponding refinement of the spatial mesh. Indeed, procedures for time step selection often advise against reducing time steps far below the critical values for temporal stability [5, p. 510]. Nevertheless, small time steps are often necessary in practice, for example in problems of radiative transport [6] and fluid-structure interaction [7]. As the time step is reduced with a fixed mesh size, the deleterious effects of higher modes are inevitably admitted into the computation, even with algorithmic damping [8]. Thus, spurious spatial oscillations may pollute the solution, at small time steps, of all

algorithms that converge in time to consistent semidiscrete formulations.

The principle of causality in classical mechanics states that cause precedes its effect. With relation to computation of discontinuous elastodynamic phenomena, numerical solutions may be polluted by spurious oscillations resulting from the sharp gradient at the front of a stress wave. Spurious oscillations arising before the wave front are noncausal. Specifically, computation of discontinuous phenomena with the trapezoidal rule is accompanied by spurious oscillations, due to its lack of algorithmic damping. At relatively large time steps these oscillations follow the wave front, but for small time steps the oscillations *precede* the wave front, violating the principle of causality. The HHT-$\alpha$ [3] and generalized-$\alpha$ [4] algorithms significantly reduce the spurious oscillations observed in the trapezoidal rule. Nonetheless spurious oscillations precede the wave front at small time steps.

An alternative approach to the method of lines is the Rothe method [9] (or horizontal method of lines) of first discretizing in time and then in space on each discrete time level. The Rothe method is employed in order to characterize the onset of noncausal oscillations and eliminate them. This method reveals that the time-discrete equation, that is solved at each time level of standard implicit schemes, can be viewed as a Galerkin approximation of a steady reaction–diffusion equation governed by a modified Helmholtz operator. An analogy to such singularly perturbed elliptic problem provides a threshold for the onset of small time step oscillations. Numerical computations obtained for smaller time steps might produce noncausal oscillations.

Any scheme that stabilizes the singularly perturbed equation removes this pathology. We propose a simple procedure of spatial stabilization, which leads to implicit time-integration schemes that are free of noncausal oscillations, without effecting unconditional temporal stability. A stabilized method for the Rothe representation is obtained by appending to its Galerkin equation residuals of its Euler–Lagrange equation in adjoint least-squares form. These residuals are multiplied by a mesh-dependent stability parameter, which is defined by von Neumann analysis. The stabilized method of adjoint type, originally called the unusual stabilized finite element method [10] and also subgrid modeling [11] or multiscale stabilization [12], may be derived in the variational multiscale framework [13], and is related to residual-free bubbles [14,15]. In practice, for the self-adjoint operators considered herein, this method is equivalent to Galerkin/least-squares, which is often employed for such problems [16].

As mentioned previously, it is well known that effects of higher modes are inevitably admitted into the computation as the time step is reduced with a fixed mesh size. The objective of this paper is to characterize the onset of instability and propose a stabilization procedure for eliminating this pathology from implicit time-integration schemes for elastodynamics. Similar work was done for the diffusion equation, as a model for parabolic problems [17]. In this paper, the equation of motion is considered as a model for hyperbolic problems.

The remainder of this paper is organized as follows. In Section 2 we consider the Newmark time-integration method for the semidiscrete equation of motion, and demonstrate the existence of noncausal oscillations at small time steps. Improved methods, such as the generalized-$\alpha$ method, concentrate on enhancement of the algorithmic damping capabilities, which can only reduce the nonphysical behavior rather than eliminate it. An alternative approach to the derivation of the time-discrete equations shows, in Section 3, that a steady reaction–diffusion model explains the pathologies observed, characterizes the threshold of instability and leads to a stabilization procedure. By analogy to the simple reaction–diffusion model, these measures are employed to derive a bound for the time step under which noncausal oscillations are expected, and then remove the instabilities from implicit time-integration schemes by spatial stabilization. Conclusions are offered in Section 4.

## 2. Formulations for elastodynamics

The equation of motion is considered as a model of a hyperbolic partial differential equation. We examine the Newmark and generalized-$\alpha$ families of time-integration schemes, although other algorithms can be considered as well.

### 2.1. Semidiscrete formulation of the equation of motion

Let $\Omega \subset \mathbb{R}^d$ be a $d$-dimensional, open, bounded domain with smooth boundary $\Gamma$. The open time interval is $(0, T)$.

Consider the following homogeneous, Dirichlet, elastodynamic problem of finding the displacement $\boldsymbol{u}(\boldsymbol{x}, t)$, such that

$$\rho \boldsymbol{u}_{,tt} - \nabla \cdot (\boldsymbol{c} \nabla \boldsymbol{u}) = \boldsymbol{f} \quad \text{in } \Omega \times (0, T), \tag{1}$$

$$\boldsymbol{u} = \boldsymbol{0} \quad \text{on } \Gamma \times (0, T), \tag{2}$$

$$\boldsymbol{u}(\boldsymbol{x}, 0) = \boldsymbol{u}_0(\boldsymbol{x}), \quad \boldsymbol{x} \in \Omega, \tag{3}$$

$$\boldsymbol{u}_{,t}(\boldsymbol{x}, 0) = \dot{\boldsymbol{u}}_0(\boldsymbol{x}), \quad \boldsymbol{x} \in \Omega. \tag{4}$$

Here, $\rho(\boldsymbol{x}) > 0$ is the known density, $\boldsymbol{c}(\boldsymbol{x})$ is the known fourth-rank tensor of elastic coefficients (with the usual symmetry and positive-definiteness properties), $\boldsymbol{f}(\boldsymbol{x}, t)$ is the prescribed body force, $\boldsymbol{u}_0(\boldsymbol{x})$ is the specified initial displacement, and $\dot{\boldsymbol{u}}_0(\boldsymbol{x})$ is the specified initial velocity. Generalization of the following results to problems with other types of boundary conditions is straightforward (see Section 2.4 for a numerical example with other types of boundary conditions).

For isotropic materials, the tensor $\boldsymbol{c}(\boldsymbol{x})$ has only two independent parameters, e.g., the Lamé parameters, $\lambda$ and $\mu$. The problem parameters can be combined in terms of the pressure and shear wave velocities, $c_L$ and $c_T$, respectively, where $c_L^2 = (\lambda + 2\mu)/\rho$ and $c_T^2 = \mu/\rho$.

Let $\Omega$ be partitioned, in the usual way, into nonoverlapping element domains, numbered with index $e$. The semidiscrete Galerkin approximation is stated in terms of a set of functions that do not depend on time $\mathscr{V}^h \subset H_0^1(\Omega)$. The standard finite element method consists of finding $\boldsymbol{u}^h(t) \in \mathscr{V}^h$,

such that $\forall \bar{\boldsymbol{u}}^h \in \mathscr{V}^h$

$$(\bar{\boldsymbol{u}}^h, \rho\ddot{\boldsymbol{u}}^h) + a(\bar{\boldsymbol{u}}^h, \boldsymbol{u}^h) = (\bar{\boldsymbol{u}}^h, \boldsymbol{f}), \tag{5}$$

$$(\bar{\boldsymbol{u}}^h, \rho\boldsymbol{u}^h(0)) = (\bar{\boldsymbol{u}}^h, \rho\boldsymbol{u}_0), \tag{6}$$

$$(\bar{\boldsymbol{u}}^h, \rho\dot{\boldsymbol{u}}^h(0)) = (\bar{\boldsymbol{u}}^h, \rho\dot{\boldsymbol{u}}_0). \tag{7}$$

Here, $\boldsymbol{x}$ is suppressed as an argument of $\boldsymbol{u}$, the superposed dot denotes time differentiation, and $(\cdot,\cdot)$ is the $L_2(\Omega)$ inner product. The form of the right-hand side assumes sufficiently smooth $\boldsymbol{f}$. The bilinear operator is

$$a(\bar{\boldsymbol{u}}, \boldsymbol{u}) = (\nabla\bar{\boldsymbol{u}}, \boldsymbol{c}\nabla\boldsymbol{u}). \tag{8}$$

The matrix equations are obtained in the usual way (see, e.g., Ref. [5]). The functions $\bar{\boldsymbol{u}}^h$ and $\boldsymbol{u}^h$ are expressed in terms of standard finite element shape functions which are not time dependent, whereas the unknown nodal displacements are time dependent.

The semidiscrete form of the initial/boundary-value problem governed by the equation of motion (1) is the well-known initial-value problem of finding the vector of unknown nodal displacements, $\mathbf{d} = \mathbf{d}(t)$, satisfying the coupled system of ordinary differential equations

$$\mathbf{M}\ddot{\mathbf{d}} + \mathbf{C}\dot{\mathbf{d}} + \mathbf{K}\mathbf{d} = \mathbf{F}, \tag{9}$$

and initial conditions

$$\mathbf{d}(0) = \mathbf{d}_0, \tag{10}$$

$$\dot{\mathbf{d}}(0) = \dot{\mathbf{d}}_0. \tag{11}$$

Here, $\mathbf{M}$ is the symmetric, positive-definite, mass matrix obtained from the first term on the left-hand side of Eq. (5); $\mathbf{C}$ is a viscous damping matrix, which is not derived from the equation of motion (1), but is often used in structural dynamics; $\mathbf{K}$ is the symmetric, positive-semidefinite, stiffness matrix obtained from the second term on the left-hand side of Eq. (5); and $\mathbf{F} = \mathbf{F}(t)$ is the prescribed force vector obtained from the right-hand side of Eq. (5). The initial conditions $\mathbf{d}_0$ and $\dot{\mathbf{d}}_0$ are usually taken as nodal values of the given functions $\boldsymbol{u}_0(\boldsymbol{x})$ and $\dot{\boldsymbol{u}}_0(\boldsymbol{x})$, respectively. The global arrays $\mathbf{M}$, $\mathbf{C}$, $\mathbf{K}$ and $\mathbf{F}$ are assembled from element arrays $\mathbf{m}^e$, $\mathbf{c}^e$, $\mathbf{k}^e$ and $\mathbf{f}^e$ in the usual way (see, e.g., Ref. [5]).

### 2.2. The Newmark method

The Newmark method for integrating the semidiscrete equation (9) from time level $t_n$ to $t_{n+1} = t_n + \Delta_t$ is expressed in terms of $\mathbf{d}_n$, $\mathbf{v}_n$ and $\mathbf{a}_n$, the approximations to $\mathbf{d}(t_n)$, $\dot{\mathbf{d}}(t_n)$ and $\ddot{\mathbf{d}}(t_n)$, respectively, as follows:

$$\mathbf{M}\mathbf{a}_{n+1} + \mathbf{C}\mathbf{v}_{n+1} + \mathbf{K}\mathbf{d}_{n+1} = \mathbf{F}_{n+1}, \tag{12}$$

$$\mathbf{d}_{n+1} = \tilde{\mathbf{d}}_{n+1} + \beta\Delta_t^2\mathbf{a}_{n+1}, \tag{13}$$

$$\mathbf{v}_{n+1} = \tilde{\mathbf{v}}_{n+1} + \gamma\Delta_t\mathbf{a}_{n+1}, \tag{14}$$

where $\Delta_t$ is the time step and the predictors are

$$\tilde{\mathbf{d}}_{n+1} = \mathbf{d}_n + \Delta_t\mathbf{v}_n + \frac{\Delta_t^2}{2}(1-2\beta)\mathbf{a}_n, \tag{15}$$

$$\tilde{\mathbf{v}}_{n+1} = \mathbf{v}_n + \Delta_t(1-\gamma)\mathbf{a}_n. \tag{16}$$

The Newmark algorithms are a one-step, two-parameter ($\beta$ and $\gamma$) family of methods. The second-order accurate, unconditionally stable in time, trapezoidal or average acceleration rule ($\beta = \frac{1}{4}$, $\gamma = \frac{1}{2}$) is, probably, the most common implicit scheme among the Newmark algorithms. The trapezoidal rule lacks algorithmic damping, which can be obtained by increasing the value of the parameter $\gamma$ beyond $\frac{1}{2}$. While this introduces the desired high-frequency dissipation, it also affects the low-frequency range, resulting in first-order accurate schemes. There is no second-order accurate Newmark method with algorithmic damping.

The following form of implementation is considered:

$$(\mathbf{M} + \gamma\Delta_t\mathbf{C} + \beta\Delta_t^2\mathbf{K})\mathbf{a}_{n+1} = \mathbf{F}_{n+1} - \mathbf{C}\tilde{\mathbf{v}}_{n+1} - \mathbf{K}\tilde{\mathbf{d}}_{n+1}. \tag{17}$$

The initialization of the solution procedure is standard. At the beginning of each time step, the terms on the right-hand side of Eq. (17) are known. The equation is solved for $\mathbf{a}_{n+1}$, and $\mathbf{d}_{n+1}$ and $\mathbf{v}_{n+1}$ are then obtained from the update equations (13) and (14).

### 2.3. The generalized-α method

Consider the integration of the semidiscrete equation (9) by the generalized-α method for second-order systems [4]. The update equations of the Newmark method (13) and (14) are retained, whereas the time-discrete equation is modified:

$$\mathbf{M}\mathbf{a}_{n+1-\alpha_m} + \mathbf{C}\mathbf{v}_{n+1-\alpha_f} + \mathbf{K}\mathbf{d}_{n+1-\alpha_f} = \mathbf{F}_{n+1-\alpha_f}, \tag{18}$$

$$\mathbf{d}_{n+1-\alpha_f} = \tilde{\mathbf{d}}_{n+1-\alpha_f} + \beta\Delta_t^2(1-\alpha_f)\mathbf{a}_{n+1}, \tag{19}$$

$$\mathbf{v}_{n+1-\alpha_f} = \tilde{\mathbf{v}}_{n+1-\alpha_f} + \gamma\Delta_t(1-\alpha_f)\mathbf{a}_{n+1}, \tag{20}$$

$$\mathbf{a}_{n+1-\alpha_m} = (1-\alpha_m)\mathbf{a}_{n+1} + \alpha_m\mathbf{a}_n, \tag{21}$$

where $t_{n+1-\alpha_f} = (1-\alpha_f)t_{n+1} + \alpha_f t_n = t_{n+1} - \alpha_f\Delta_t$. The predictors are

$$\tilde{\mathbf{d}}_{n+1-\alpha_f} = \mathbf{d}_n + \Delta_t(1-\alpha_f)\mathbf{v}_n + \frac{\Delta_t^2}{2}(1-2\beta)(1-\alpha_f)\mathbf{a}_n, \tag{22}$$

$$\tilde{\mathbf{v}}_{n+1-\alpha_f} = \mathbf{v}_n + \Delta_t(1-\gamma)(1-\alpha_f)\mathbf{a}_n. \tag{23}$$

The generalized-α method is an extension of the Newmark method that exhibits algorithmic damping. It is defined in terms of parameters $\alpha_m$ and $\alpha_f$, in addition to $\beta$ and $\gamma$. Selecting $\alpha_m = \alpha_f = 0$ leads to the familiar Newmark family of methods. Selecting $\alpha_m = 0$, $\alpha_f = -\alpha$ leads to the HHT-α method [3].

Alternatively, selecting

$$\alpha_m = \frac{2\rho_\infty - 1}{\rho_\infty + 1}, \tag{24}$$

$$\alpha_f = \frac{\rho_\infty}{\rho_\infty + 1}, \tag{25}$$

$$\beta = (1 - \alpha_m + \alpha_f)^2/4, \tag{26}$$

$$\gamma = (1 - 2\alpha_m + 2\alpha_f)/2, \tag{27}$$

defines an unconditionally stable in time, second-order accurate, one-parameter ($0 \leqslant \rho_\infty \leqslant 1$), family of methods. The parameter $\rho_\infty$ specifies the dissipation of the high-frequency modal components. Taking $\rho_\infty = 0$ eliminates the high-frequency response (known as asymptotic annihilation). On the other extreme, setting $\rho_\infty = 1$ eliminates the algorithmic damping and the trapezoidal time-integration scheme is regained.

The following form of implementation is considered:

$$\begin{aligned}&((1-\alpha_m)\mathbf{M} + \gamma\Delta_t(1-\alpha_f)\mathbf{C} + \beta\Delta_t^2(1-\alpha_f)\mathbf{K})\mathbf{a}_{n+1} \\ &\quad = \mathbf{F}_{n+1-\alpha_f} - \alpha_m\mathbf{M}\mathbf{a}_n - \mathbf{C}\tilde{\mathbf{v}}_{n+1-\alpha_f} - \mathbf{K}\tilde{\mathbf{d}}_{n+1-\alpha_f}.\end{aligned} \tag{28}$$

Again, the initialization of the solution procedure is standard. At the beginning of each time step, the terms on the right-hand side of Eq. (28) are known. The equation is solved for $\mathbf{a}_{n+1}$, and then $\mathbf{d}_{n+1}$ and $\mathbf{v}_{n+1}$ are obtained using the update equations of the Newmark method (13) and (14)

$$\mathbf{d}_{n+1} = \frac{\tilde{\mathbf{d}}_{n+1-\alpha_f} - \alpha_f\mathbf{d}_n + \beta\Delta_t^2(1-\alpha_f)\mathbf{a}_{n+1}}{1-\alpha_f}, \tag{29}$$

$$\mathbf{v}_{n+1} = \frac{\tilde{\mathbf{v}}_{n+1-\alpha_f} - \alpha_f\mathbf{v}_n + \gamma\Delta_t(1-\alpha_f)\mathbf{a}_{n+1}}{1-\alpha_f}. \tag{30}$$

### *2.4. Motivation: numerical example*

Consider a one-dimensional wave propagation problem in a uniform bar of length $L$ and a constant bar wave velocity $c_0 = \sqrt{E/\rho}$, where $E$ is Young's modulus and $\rho$ is the material density. The model lacks physical damping. No body force is applied. The bar is fixed on the left end, and a constant pressure $p$ is applied at $t = 0$ on the right end (see Fig. 1). The bar is initially at rest. Once the load is applied, a stress wave is generated, propagating towards the fixed end at the bar wave velocity $c_0$. Attention is restricted to the time interval before the stress wave reaches the fixed end of the bar ($T < L/c_0$).

The initial/boundary-value problem is

$$\ddot{u} - c_0^2 u'' = 0, \quad 0 < x < L, \;\; 0 < t < T, \tag{31}$$

$$u(0,t) = 0, \quad 0 < t < T, \tag{32}$$

$$\sigma(L,t) = p, \quad 0 < t < T, \tag{33}$$

$$u(x,0) = 0, \quad 0 < x < L, \tag{34}$$

$$\dot{u}(x,0) = 0, \quad 0 < x < L, \tag{35}$$

where $\sigma = Eu'$.

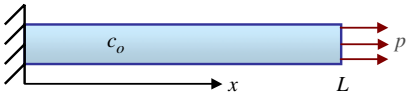


Fig. 1. Bar fixed on the left end and subject to pressure on the right end.

The exact solution is [18, p. 91]

$$u = \frac{p}{E}\langle c_0 t - (L - x)\rangle, \tag{36}$$

where $\langle\cdot\rangle$ is the Macaulay bracket. The bar is at rest before the wave front, since the stress wave has not yet arrived due to the finite velocity of propagation, conforming to the principle of causality. The discretization error inherent in numerical methods invariably leads to precursors before wave fronts that violate the principle of causality. Such precursors are considered acceptable as long as they are monotonic and small. Numerical solutions may also exhibit spurious oscillations on both sides of the wave front resulting from sharp gradients in stress. Noncausal oscillations, appearing before the wave front, are inappropriate.

Numerical computations were performed using a uniform mesh of 100 linear rod elements ($h = L/100$) and three time steps CFL $= 1.0, 0.5, 0.1$, where CFL $= c_0\Delta_t/h$ is the Courant number. Recall, CFL $= 1$ is the critical time step for temporal stability of the central difference method ($\beta = 0$, $\gamma = \frac{1}{4}$), the explicit scheme of the Newmark method (when the mass matrix is lumped).

Snapshots of the numerical solutions for the stress, obtained by the trapezoidal rule and generalized-$\alpha$ method ($\rho_\infty = \frac{7}{13}$) at $t = 0.6L/c_0$, are shown in Fig. 2. The numerical solutions exhibit spurious oscillations resulting from sharp gradients at the wave front. For the largest time step (CFL $= 1.0$), the solutions exhibit small monotonic precursors but are free of noncausal oscillations, as can be seen in Fig. 2(a). For the trapezoidal rule, spurious oscillations follow the wave front. The damping property of the generalized-$\alpha$ method is apparent. For the medium time step (CFL $= 0.5$), the onset of spurious oscillations *before* the wave front can be observed in Fig. 2(b), violating the principle of causality. Again, the damping property of the generalized-$\alpha$ method is evident, but still noncausal oscillations exist. For the smallest time step (CFL $= 0.1$), the spurious oscillations before the wave front are no longer localized, as is the case for the medium time step, as can be seen in Fig. 2(c). At this time step, the solutions are essentially converged to the solution of the semidiscrete formulation, hence the two solutions are almost identical.

## 3. Spatial stability analysis

The numerical example in the previous section shows that standard time-integration schemes exhibit noncausal phenomena at small time steps. These pathologies can be explained by examining a simple free-space model. Furthermore, this model can be used to formulate stabilized methods that are free of

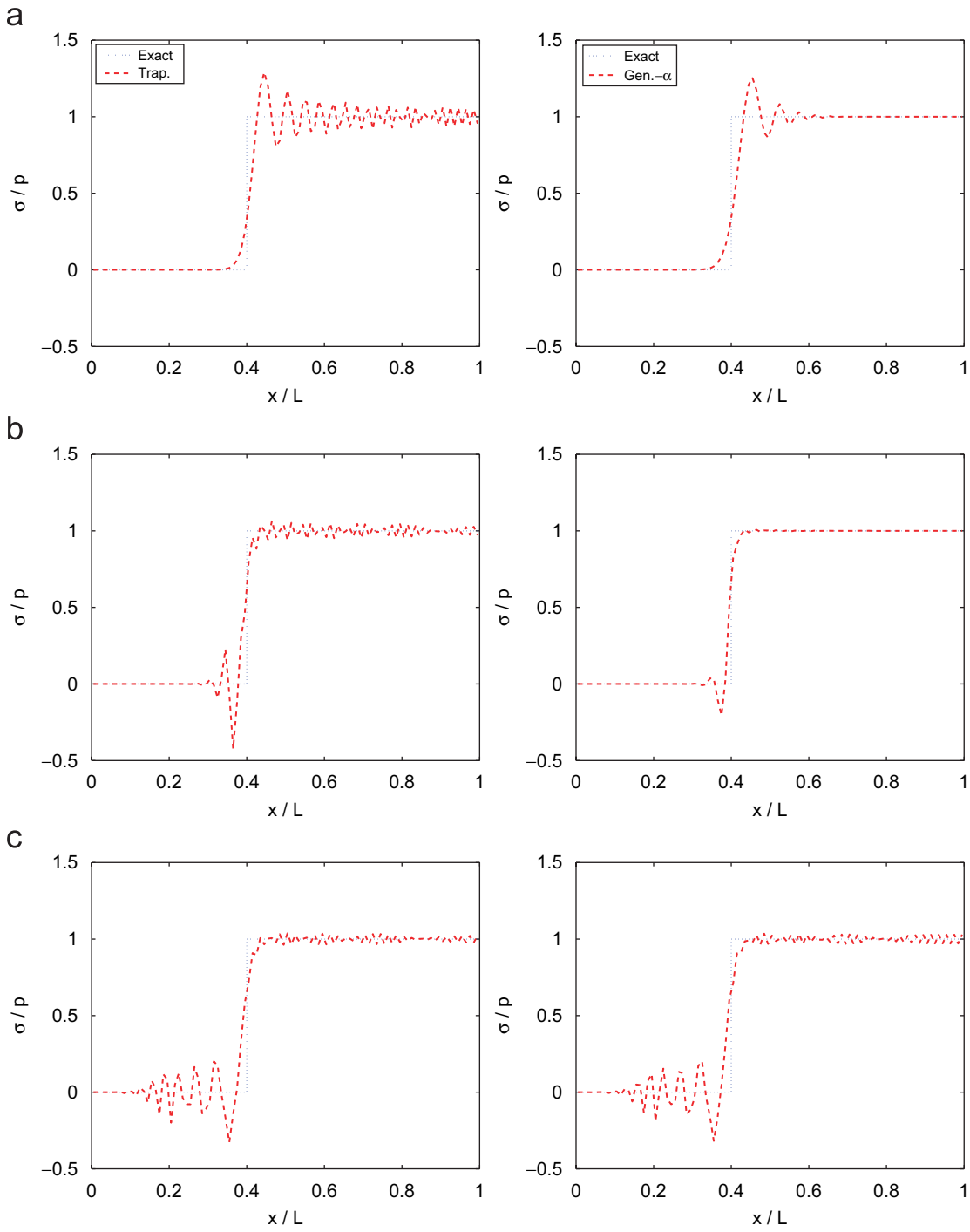


Fig. 2. Snapshots of stress computed by the trapezoidal rule and generalized-α method ($\rho_\infty = \frac{7}{13}$) at $t = 0.6L/c_0$ (compared to the exact solution). (a) Solutions at CFL = 1.0: trapezoidal rule (left) and generalized-α method (right). (b) Solutions at CFL = 0.5: trapezoidal rule (left) and generalized-α method (right). (c) Solutions at CFL = 0.1: trapezoidal rule (left) and generalized-α method (right).

noncausal oscillations at all time steps. Consider the scalar wave equation

$$\ddot{u} - c^2 \Delta u = f, \tag{37}$$

where $c$ is the appropriate wave velocity (e.g., $c_T$, $c_L$ or $c_0$).

### *3.1. Time-integration by the Newmark method*

By the Rothe method, the space–time continuous wave equation (37) is discretized in time by the Newmark time-integration scheme in terms of $u_n(x)$, $v_n(x)$ and $a_n(x)$, the approximations at time $t_n$ to $u(x,t)$, $\dot{u}(x,t)$ and $\ddot{u}(x,t)$,

respectively, as follows:

$$a_{n+1} - c^2 \Delta u_{n+1} = f(x, t_{n+1}), \tag{38}$$

$$u_{n+1} = \tilde{u}_{n+1} + \beta \Delta_t^2 a_{n+1}, \tag{39}$$

$$v_{n+1} = \tilde{v}_{n+1} + \gamma \Delta_t a_{n+1}, \tag{40}$$

where the predictors are

$$\tilde{u}_{n+1} = u_n + \Delta_t v_n + \frac{\Delta_t^2}{2}(1 - 2\beta) a_n, \tag{41}$$

$$\tilde{v}_{n+1} = v_n + \Delta_t (1 - \gamma) a_n. \tag{42}$$

Substitution leads to the following steady reaction–diffusion equation

$$\mathscr{L} a_{n+1} = \tilde{f}, \tag{43}$$

where $\mathscr{L} u = -\beta \Delta_t^2 c^2 \Delta u + u$ is a modified Helmholtz operator and $\tilde{f} = f(x, t_{n+1}) + c^2 \Delta \tilde{u}_{n+1}$. The degradation of stability for this singularly perturbed elliptic equation at small values of the parameter is well-known.

### *3.1.1. Stability of spatial Galerkin approximation*

The Galerkin approximation of the free-space model (neglecting boundary conditions) consists of finding $a_{n+1}^h$, such that

$$(\bar{a}_{n+1}^h, a_{n+1}^h) + a(\bar{a}_{n+1}^h, a_{n+1}^h) = (\bar{a}_{n+1}^h, \tilde{f}). \tag{44}$$

In order to recover the usual discrete form, the predictor term on the right-hand side should be integrated by parts. The bilinear operator in this case is

$$a(\bar{u}, u) = \beta \Delta_t^2 (\nabla \bar{u}, c^2 \nabla u). \tag{45}$$

Free-space solutions of the constant-coefficient, homogeneous, reaction–diffusion equation exhibit exponential growth and decay with rate $1/(\sqrt{\beta}\Delta_t c)$, which is related to the Courant number (CFL) in computation. Von Neumann analysis of the Galerkin method of a uniform $d$-dimensional mesh of linear elements of size $h$ aligned with the direction of growth or decay leads to an expression for the approximate growth or decay rate (for more details, see Ref. [17]). Expressing the approximate exponential rate as $\mathrm{CFL}^h$, the Galerkin method results in the following relation:

$$\frac{1}{\mathrm{CFL}^h} = \sqrt{\beta}\ \mathrm{arccosh}\left(\frac{6\beta\,\mathrm{CFL}^2 + 2}{6\beta\,\mathrm{CFL}^2 - 1}\right). \tag{46}$$

This expression represents the correct behavior of exponential growth and decay ($\mathrm{CFL}^h \in \mathbb{R}$) when $\mathrm{CFL}^2 > 1/(6\beta)$. For $\mathrm{CFL} < 1/\sqrt{6\beta}$, $\mathrm{CFL}^h$ is complex valued, which represents spurious oscillations. This is a manifestation of degradation of spatial stability of the time-discrete problem, in the $H^1$ sense, as the value of the CFL decreases, while maintaining $L_2$ stability, which is incapable of controlling derivatives. Considerable degradation in accuracy is possible (Fig. 3) even prior to the potential onset of spurious oscillations at $\mathrm{CFL} = 1/\sqrt{6\beta}$.

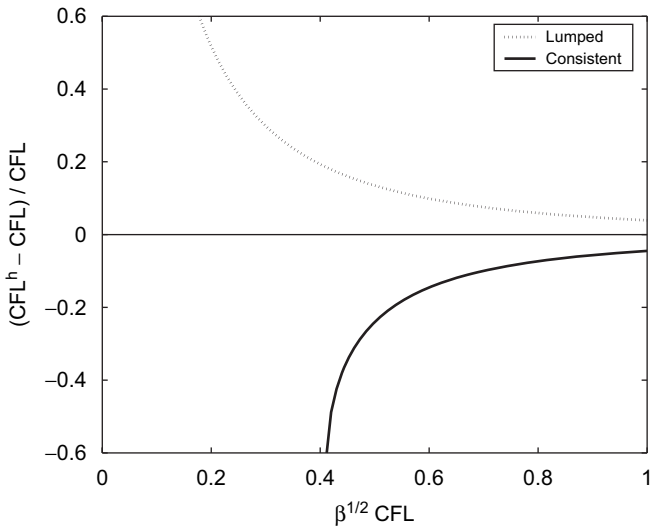


Fig. 3. Error in growth and decay rate for the Galerkin method (solid line) and for lumped mass method (dotted line) prior to potential onset of spurious oscillations.

**Remark 1.** This analysis holds for consistent representation of inertial terms. With lumped mass, the expression for the approximate growth and decay rate becomes

$$\frac{1}{\mathrm{CFL}^h} = \sqrt{\beta}\ \mathrm{arccosh}\left(1 + \frac{1}{2\beta\,\mathrm{CFL}^2}\right). \tag{47}$$

This relation represents exponential growth and decay for all admissible values of $\sqrt{\beta}\,\mathrm{CFL}$, and hence solutions are free of spurious oscillations (see Fig. 3). However, this may not be the case for lumped mass elements of high-order. For the linear elements considered here, the error of the approximate growth and decay rate, related to the local truncation error, is of the same order as in the consistent representation on uniform meshes. The consistent representation retains second-order spatial accuracy in the local truncation error on non-uniform meshes, whereas the lumped representation can degrade to first order [19]. Moreover, the loss of guaranteed bounds, when the variational framework is violated by mass lumping, can be detrimental to the use of techniques such as error estimation.

In summary, the Galerkin solution with linear elements may exhibit spurious spatial oscillations for

$$\mathrm{CFL} < \frac{1}{\sqrt{6\beta}}, \tag{48}$$

and considerable degradation in accuracy even prior to the potential onset of the spurious oscillations. Note that the bound for the time step is $O(h)$. For the trapezoidal rule ($\beta = \frac{1}{4}, \gamma = \frac{1}{2}$), the bound for spatial stability is $\mathrm{CFL} < \sqrt{\frac{2}{3}}$.

### *3.1.2. Stabilized method*

A stabilized finite element method for the Newmark algorithm is obtained by appending to the Galerkin equation (44)

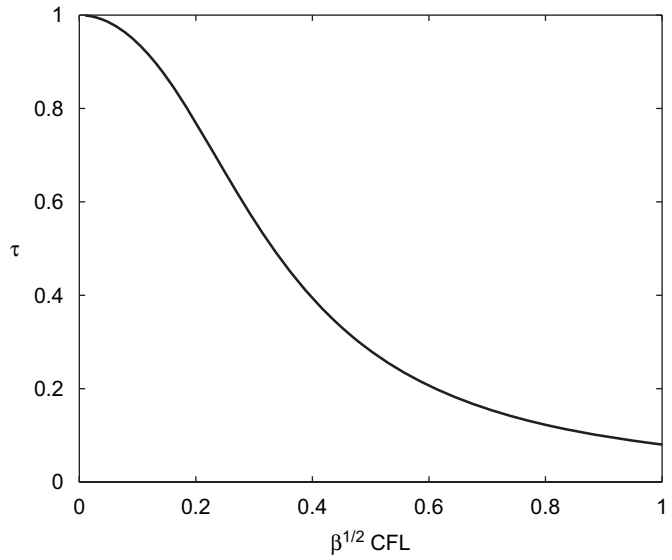


Fig. 4. Stabilization parameter for linear elements.

terms containing residual-based operators multiplied by method parameters $\tau$:

$$(\bar{a}^h_{n+1}, a^h_{n+1}) + a(\bar{a}^h_{n+1}, a^h_{n+1}) - (\mathscr{L}^*\bar{a}^h_{n+1}, \tau\mathscr{L}a^h_{n+1})_{\widetilde{\Omega}} = (\bar{a}^h_{n+1}, \tilde{f}) - (\mathscr{L}^*\bar{a}^h_{n+1}, \tau\tilde{f})_{\widetilde{\Omega}}, \tag{49}$$

where $\mathscr{L}^*$ is the adjoint operator of the differential operator $\mathscr{L}$ given in Eq. (43). The mesh-dependent stabilization parameter for linear elements of size $h$,

$$\tau = 1 + 6\beta\,\mathrm{CFL}^2\,\frac{1-\cosh(1/(\sqrt{\beta}\,\mathrm{CFL}))}{2+\cosh(1/(\sqrt{\beta}\,\mathrm{CFL}))}, \tag{50}$$

is defined on the element level. We note for later reference that $0 \leqslant \tau < 1$ for $\sqrt{\beta}\,\mathrm{CFL} > 0$ (see Fig. 4).

Subscripts on inner products denote domains of integration other than $\Omega$, namely, $\widetilde{\Omega}$ denotes the union of element interiors such that $\overline{\Omega} = \overline{\widetilde{\Omega}}$. Integration of the additional terms is performed over $\widetilde{\Omega}$ in order to respect regularity requirements of typical, piecewise smooth, finite element functions. In practice, standard finite element procedures which assemble global arrays from element contributions are employed without modification. For linear elements, spatial stabilization is obtained by a simple modification of the element mass matrix and force vector prior to assembly, namely

$$\mathbf{m}^e \leftarrow (1-\tau)\mathbf{m}^e, \tag{51}$$

$$\mathbf{f}^e \leftarrow (1-\tau)\mathbf{f}^e. \tag{52}$$

Recall, the predictor terms in the force vector are integrated by parts.

Symmetry of the spatially stabilized mass matrix follows directly from the definition of the modified matrix. Positive-definiteness of the modified mass matrix follows along the lines of the procedure for the original matrix, recalling that $1-\tau > 0$. The analysis of the spatially stabilized Newmark method is similar to that of the conventional method [5, pp. 497–498], indicating that spatial stabilization does not effect unconditional temporal stability.

Repeating the analysis in Section 3.1.1 for the stabilized method (49) shows that setting the method parameter as (50) leads to $\mathrm{CFL}^h = \mathrm{CFL}$, eliminating errors in the exponential rate in Cartesian meshes of linear elements aligned in the direction of growth and decay, along with the attendant spurious oscillations. Stabilization restores the correct balance between the $L_2$ and $H^1$ terms. Furthermore, it reduces the sensitivity of the computation to spurious phenomena that are generated by transitions in mesh size [20].

### *3.2. Time-integration by the generalized-α method*

The wave equation (37) is now discretized, by the Rothe method, with the generalized-α time-integration scheme, as follows:

$$a_{n+1-\alpha_m} - c^2\Delta u_{n+1-\alpha_f} = f(x, t_{n+1-\alpha_f}), \tag{53}$$

$$u_{n+1-\alpha_f} = (1-\alpha_f)u_{n+1} + \alpha_f u_n, \tag{54}$$

$$v_{n+1-\alpha_f} = (1-\alpha_f)v_{n+1} + \alpha_f v_n, \tag{55}$$

$$a_{n+1-\alpha_m} = (1-\alpha_m)a_{n+1} + \alpha_m a_n, \tag{56}$$

where

$$u_{n+1} = \frac{\tilde{u}_{n+1-\alpha_f} - \alpha_f u_n + \beta\Delta_t^2(1-\alpha_f)a_{n+1}}{1-\alpha_f}, \tag{57}$$

$$v_{n+1} = \frac{\tilde{v}_{n+1-\alpha_f} - \alpha_f v_n + \gamma\Delta_t(1-\alpha_f)a_{n+1}}{1-\alpha_f} \tag{58}$$

and

$$\tilde{u}_{n+1-\alpha_f} = u_n + \Delta_t(1-\alpha_f)v_n + \frac{\Delta_t^2}{2}(1-2\beta)(1-\alpha_f)a_n, \tag{59}$$

$$\tilde{v}_{n+1-\alpha_f} = v_n + \Delta_t(1-\gamma)(1-\alpha_f)a_n. \tag{60}$$

As in the case of the Newmark method, simple manipulation yields a steady reaction–diffusion equation for $a_{n+1}$. Eq. (43) is regained with $\mathscr{L}u = -((1-\alpha_f)/(1-\alpha_m))\beta\Delta_t^2c^2\Delta u + u$, the modified Helmholtz operator, and $\tilde{f} = f(x, t_{n+1-\alpha_f}) - \alpha_m a_n + c^2\Delta\tilde{u}_{n+1-\alpha_f}$. Once again, the predictor term of $\tilde{f}$ is integrated by parts in the weak form.

Repeating the analysis in Section 3.1.1 leads to a bound for the time step, under which noncausal spatial oscillations may occur. Specifically, noncausal spatial oscillations may arise in the standard one-parameter ($\rho_\infty$) family of generalized-α methods for

$$\mathrm{CFL} < (1+\rho_\infty)\sqrt{\frac{2-\rho_\infty}{6}}. \tag{61}$$

Again, the bound for the time step is $O(h)$. Recall, the parameter $\rho_\infty$ specifies the dissipation of the high-frequency

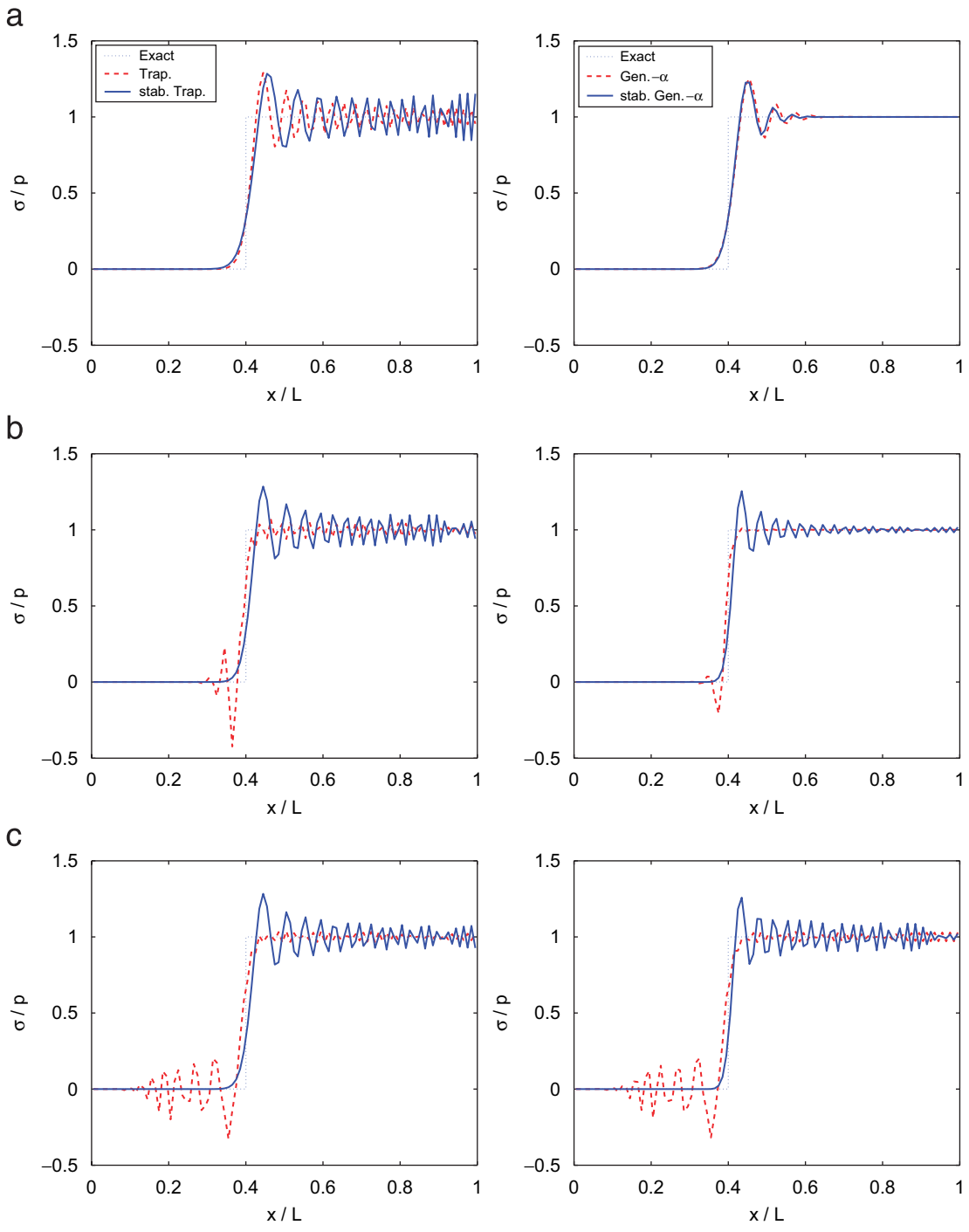


Fig. 5. Snapshots of stress computed by the stabilized trapezoidal rule and stabilized generalized-α method ($\rho_\infty = \frac{7}{13}$) at $t = 0.6L/c_0$ (compared to the exact and unstabilized solutions). (a) Solutions at CFL = 1.0: stabilized trapezoidal rule (left) and stabilized generalized-α method (right). (b) Solutions at CFL = 0.5: stabilized trapezoidal rule (left) and stabilized generalized-α method (right). (c) Solutions at CFL = 0.1: stabilized trapezoidal rule (left) and stabilized generalized-α method (right).

modal components. Setting $\rho_\infty = 1$, eliminating the algorithmic damping, recovers the bound for spatial stability of the trapezoidal time-integration scheme CFL $< \sqrt{\frac{2}{3}}$. On the other extreme, taking $\rho_\infty = 0$, eliminating the high-frequency response, improves the bound for spatial stability CFL $< \sqrt{\frac{1}{3}}$ compared to the trapezoidal rule. For $\rho_\infty = \frac{7}{13}$ (from the numerical example) the bound for spatial stability is CFL $< 0.76$.

A stabilized version of the generalized-α algorithm is obtained by the procedure outlined in Section 3.1.2. The

mesh-dependent stabilization parameter for linear elements of size $h$ in this case is obtained by substituting in Eq. (50) $1/((2-\rho_\infty)(1+\rho_\infty)^2)$ for $\beta$.

### 3.3. Numerical example revisited

Returning to the numerical example described in Section 2.4, the stability analysis, with $c_0$ as the appropriate wave velocity, shows that the largest time step (CFL = 1.0) is higher than the bounds for spatial stability (48) and (61) for both algorithms considered ($\beta=\frac{1}{4}$, $\rho_\infty=\frac{7}{13}$). Indeed, the solutions for the largest time step are free of noncausal oscillations (see Fig. 2(a)). On the other hand, the medium time step (CFL = 0.5) is a little below and the smallest time step (CFL = 0.1) is well below these bounds, explaining the noncausal oscillations observed in Figs. 2(b) and (c).

Snapshots of the numerical solutions for the stress, obtained by the *stabilized* trapezoidal rule and *stabilized* generalized-$\alpha$ method at $t = 0.6L/c_0$, are shown in Fig. 5. The numerical solutions still exhibit spurious oscillations resulting from sharp gradients at the wave front. However, spurious oscillations before the wave front are absent from the solutions of the stabilized methods, even for time steps lower than the bounds for spatial stability (48) and (61), thus conforming to the principle of causality. The solutions of the stabilized trapezoidal rule for all three time steps are similar to the solution of the unstabilized trapezoidal rule for the largest time step. The damping property of the stabilized generalized-$\alpha$ method is apparent, providing the best performance.

While the proposed approach successfully removes noncausal oscillations from the computation, considerable spurious oscillations remain. The combination of spatial stabilization and algorithmic damping is probably incapable of addressing this deficiency, which would require combining spatial stabilization with more advanced time-marching schemes. Initialization procedures and alternative forms of implementation should also be examined.

## 4. Conclusions

Solutions of semidiscrete formulations for hyperbolic problems may exhibit noncausal oscillations, due to poor approximation of higher modes. Consequently, all conventional direct time-integration schemes that are based on such semidiscrete formulations and are convergent in time may eventually admit these pathologies as the time step is reduced (with a fixed mesh size).

In this paper, a procedure for determining specific values for the potential onset of noncausal spatial oscillations is provided by considering the scalar wave equation as a simple model. Time discretization by the Rothe method leads to a singularly perturbed, steady, reaction–diffusion equation. In particular, bounds (for linear elements) are obtained for implicit algorithms belonging to the Newmark and generalized-$\alpha$ methods.

The time-discrete problem can be stabilized by any procedure that is used for the singularly perturbed equation. For linear elements, spatial stabilization is obtained by a simple modification of the element mass matrix and force vector prior to assembly, in order to improve spatial performance within each time step. This procedure preserves the property of unconditional temporal stability. Employing spatial stabilization, as proposed, eliminates noncausal oscillations observed in implicit computations with small time steps. The best performance is obtained by a combination of spatial stabilization and algorithmic damping, as in the case of the stabilized version of the generalized-$\alpha$ method.

The onset of noncausal spatial oscillations in implicit time-integration occurs at time steps of the order of the critical time step for temporal stability of corresponding explicit schemes. Consequently, this pathology may be of particular concern in the application of implicit–explicit mesh partitions. The stabilization procedure proposed in this work is well suited for the implicit part of such algorithms.

## References


[1] I.S. Berezin, N.P. Zhidkov, Computing Methods, vols. I and II, Pergamon Press, Oxford, 1965.

[2] G. Strang, G.J. Fix, An Analysis of the Finite Element Method, Prentice-Hall, Englewood Cliffs, NJ, 1973.

[3] H.M. Hilber, T.J.R. Hughes, R.L. Taylor, Improved numerical dissipation for time integration algorithms in structural dynamics, Earthquake Eng. Struct. Dyn. 5 (1977) 282–292.

[4] J. Chung, G.M. Hulbert, A time integration algorithm for structural dynamics with improved numerical dissipation: the generalized-$\alpha$ method, Trans. ASME J. Appl. Mech. 60 (1993) 371–375.

[5] T.J.R. Hughes, The Finite Element Method, Dover Publications, Mineola, NY, 2000 (corrected reprint of the 1987 original).

[6] C.C. Ober, J.N. Shadid, Studies on the accuracy of time-integration methods for the radiation–diffusion equations, J. Comput. Phys. 195 (2) (2004) 743–772.

[7] A. Masud, Effects of mesh motion on the stability and convergence of ALE based formulations for moving boundary flows, Comput. Mech. 38 (4–5) (2006) 430–439.

[8] S. Krenk, State-space time-integration with energy control and fourth-order accuracy for linear dynamic systems, Int. J. Numer. Methods Eng. 65 (2006) 595–619.

[9] E. Rothe, Zweidimensionale parabolische Randwertaufgaben als Grenzfall eindimensionaler Randwertaufgaben, Math. Ann. 102 (1930) 650–670.

[10] L.P. Franca, S.L. Frey, T.J.R. Hughes, Stabilized finite element methods. I. Application to the advective–diffusive model, Comput. Methods Appl. Mech. Eng. 95 (2) (1992) 253–276.

[11] J.I. Cipolla, Subgrid modeling in a Galerkin method for the Helmholtz equation, Comput. Methods Appl. Mech. Eng. 177 (1–2) (1999) 35–49.

[12] T.J.R. Hughes, G.N. Wells, Conservation properties for the Gelrekin and stabilized forms of the advection–diffusion and incompressible Navier–Stokes equations, Comput. Methods Appl. Mech. Eng. 194 (9–11) (2005) 1141–1159.

[13] T.J.R. Hughes, Multiscale phenomena: Green's functions, the Dirichlet-to-Neumann formulation, subgrid scale models, bubbles and the origins of stabilized methods, Comput. Methods Appl. Mech. Eng. 127 (1–4) (1995) 387–401.

[14] F. Brezzi, M.O. Bristeau, L.P. Franca, M. Mallet, G. Rogé, A relationship between stabilized finite element methods and the Galerkin method with bubble functions, Comput. Methods Appl. Mech. Eng. 96 (1) (1992) 117–129.

[15] L.P. Franca, C. Farhat, Bubble functions prompt unusual stabilized finite element methods, Comput. Methods Appl. Mech. Eng. 123 (1–4) (1995) 299–308.

[16] I. Harari, S. Haham, Improved finite element methods for elastic waves, Comput. Methods Appl. Mech. Eng. 166 (1–2) (1998) 143–164.
[17] I. Harari, Stability of semidiscrete formulations for parabolic problems at small time steps, Comput. Methods Appl. Mech. Eng. 193 (15–16) (2004) 1491–1516.
[18] K.F. Graff, Wave Motion in Elastic Solids, Oxford University Press, Oxford, 1975.
[19] I. Harari, E. Turkel, Accurate finite difference methods for time-harmonic wave propagation, J. Comput. Phys. 119 (2) (1995) 252–270.
[20] I. Harari, Reducing spurious dispersion, anisotropy and reflection in finite element analysis of time-harmonic acoustics, Comput. Methods Appl. Mech. Eng. 140 (1–2) (1997) 39–58.